Multichannel probes for polarization-resolved scanning near-field optical microscopy

T. Grosjean, I. A. Ibrahim, Mathieu Mivelle Mivelle

Multichannel probes for polarization-resolved scanning near-field optical microscopy

Thierry Grosjean,* Idriss A. Ibrahim, and Mathieu Mivelle

Département d'Optique P.M. Duffieux, Institut FEMTO-ST, UMR CNRS 6174, Université de Franche-Comté, 16 route de Gray, 25030 Besançon cedex, France

*Corresponding author: thierry.grosjean@univ-fcomte.fr

We propose and validate a concept of multichannel near-field fiber probe for the collection and discrimination of optical fields of orthogonal polarizations (linear, elliptic, and circular). The system is achieved by connecting to scanning near-field optical microscope fiber tips an optical stage made up of commercial polarizers, fiber couplers, and polarization controllers. Using radially polarized Bessel beams as test objects, we demonstrate the ability of a three-channel fiber tip to simultaneously and independently probe the transverse vector components of the electric field (parallel to the sample surface) and the overall transverse intensity. The polarization ratio of the near-field collection system exceeds 1:1500. The system can be implemented in collection-mode or reflection-mode near-field microscope configurations, with various kinds of probe and light source (of high or low coherence lengths) for a deeper insight of light polarization effects and vector fields at a subwavelength scale.

1. Introduction

Although scanning near-field optical microscopy (SNOM) relies on the complex interaction between local probes and spatially varying 3D vector fields, it historically started by providing scalar intensity information to finer sample details [1–4]. The development of polarization contrast SNOM [5] rapidly showed that knowledge of local polarization is essential for image interpretation. Later, the concept of emission and detection of cross-polarized optical signals allowed reflection-mode SNOM (r SNOM) to improve its signal-to-noise ratio as well as its resolution, even with dielectric uncoated tips [6,7]. Polarization control and analysis in SNOM finds fruitful applications in magneto-optics and data storage [8], polarimetry [9,10], and vector field probing [11,12]. In all these experiments, a single polarization direction is analyzed per acquisition. Therefore, a detailed description of 2D or 3D polarization effects requires a multi-acquisition process that is risky both for the tip and the sample. Recently, the simultaneous detection of orthogonal transverse electric field components or out-of-plane magnetic field and one transverse electrical field component has been shown above a ridge waveguide [11]. However, the overall detection system, based on a heterodyne interferometer, is difficult to stabilize and works with light sources of high coherence lengths, which limits the panel of applications of the microscope. We show a simple and stable system for the simultaneous detection of orthogonal light field components. Depending on the probe used, various electric and/or magnetic field components can be selectively and simultaneously probed. The multichannel system can be used with light sources of low coherence lengths and can be extended to simultaneous polarization control and analysis at various wavelengths. Vectorial SNOM probing of subwavelength nonlinear optical phenomena becomes possible. Our system can also be implemented in a reflection-mode SNOM for deeper insight of polarization effects at a subwavelength scale.

2. Principle

SNOM fiber tips used in a collection mode are known to develop anisotropic sensitivities with respect to the vector optical fields. Generally, they cannot faithfully collect all the information from the various vectorial components of light fields diffracted by the sample. Some electric or magnetic components can even be filtered out by the tip itself and/or by the tip-to-fiber energy coupling process. For example, single-mode dielectric fiber tips are sensitive mainly to the electric field but are unable to collect the field component along the tip axis whereas multimode fiber tips attenuate the signal from this longitudinal field component by 90% [13,14]. It has been seen that single-mode aperture probes develop a sensitivity to the transverse electric field [15] with no sensitivity to the longitudinal field, whereas a recent theoretical study has shown that circular nano-apertures also develop a high sensitivity to the transverse magnetic field [16]. Finally, cut aperture tips can couple the longitudinal magnetic field and one transverse electric field into cross-polarized degenerated fundamental fiber modes [11]. Recent and future advances in probe design and fabrication techniques will probably allow the detection of specific optical field components on demand.

Here we propose to discriminate the collected signals from orthogonal optical field components by connecting to the fiber probe a network of optical fibers achieved by cascading single-mode polarization-insensitive fiber couplers. The overall signal that leaves the tip can thus be split into as many channels as field components and/or polarizations (linear, elliptic, or circular) that need to be discriminated. One or more channels can be added to have access to the overall signal from all the field components. Note that a network of N couplers leads to $N+1$ output channels. During image acquisition, the discrimination of the collected signals from the orthogonal field components is performed by positioning linear polarizers between the end facet of the channel outputs and the photodetectors. The use of conventional polarizers coupled to fiber probes is typical in emission- and reflection-mode SNOM for polarization contrast and polarization modulation experiments [5–7,9]. In our case, the intrinsic birefringences of the various fiber channels are finely controlled with fiber polarization controllers (Babinet–Soleil or three-paddle) to accurately define the polarization sensitivity of each channel during calibration and to maintain this sensitivity during measurements. Therefore, one can imagine a multichannel polarizing SNOM system that is sensitive to both orthogonal field components and combinations of these components that lead to circular or elliptic polarization local detections. Note that the loss of signal-to-noise ratio that is due to repeated splitting in the fiber network is the main limiting factor in image acquisition with our system, as the signal collected by a SNOM tip is usually weak; for example, it will limit the number of output channels.

3. First Realization

To validate this concept, we developed a three-output fiber network aimed at discriminating the signals collected by an uncoated single-mode fiber tip from the two transverse electric light field components (called E_x and E_y in the following); see Fig. 1. The system is engineered to work at $\lambda = 633\,\text{nm}$. The overall signal collected by the tip is split into two channels by means of a 50/50 monomode fiber coupler. One of the two output channels is connected to a detector (D_3) for direct measurement of the overall transverse intensity. The other channel is then connected to a second 50/50 monomode fiber coupler for separate detection of the signals from E_x and E_y components. The simultaneous detections of E_x and E_y are achieved by inserting high quality polarizers (P_1 and P_2), of $1:10^4$ polarization ratio, between the end facets of the fiber system and detectors D_1 and D_2. The tip is fabricated by heating and pulling a monomode fiber with a P-2000 puller from Sutter Instrument, Novato, California. Special care is taken during the fabrication procedure to ensure the desired polarization performances for the collection system. Two three-paddle type fiber polarization controllers (Fiber Control, Holmdel, New Jersey) are added to the end parts of the two polarizing channels to selectively couple to D_1 and D_2 the signals extracted by the tip from the two transverse electric field components.

The inset in Fig. 1 displays the polarization diagram of the SNOM setup. It is achieved by projecting a linearly polarized collimated beam (from a He–Ne laser) directly onto the tip. Then the power collected by the tip is measured through the two polarizing channels by detectors D_1 and D_2, while the input polarization is rotated by means of a half-wave retardation plate. Experimental values (squares and triangles) fit the ideal polarization diagrams of two orthogonal polarizers described by cosine functions (solid and dashed curves). The polarization ratios of cross-polarized channels 1 and 2 are measured

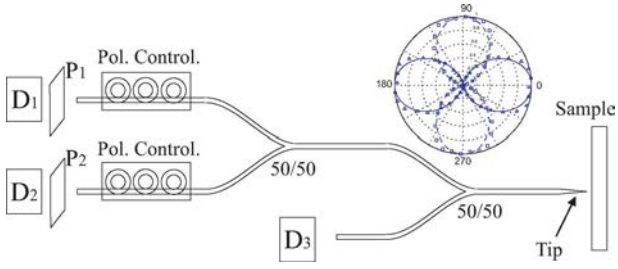

Fig. 1. (Color online) Scheme of a three-channel fiber tip. Two channels, connected to detectors D_1 and D_2, give intensity information about transverse field components E_x and E_y, respectively. The last channel measures the overall transverse intensity. Inset: collection diagram of polarizing channels 1 and 2 (associated with D_1 and D_2). Solid and dashed lines: ideal diagrams of channels 1 and 2, respectively; squares and triangles: experimental measurements for channels 1 and 2, respectively. The polarization ratio of the system is approximately 1:1500.

to values larger than 1 : 1500 (extinction ratios larger than 32 dB).

Because real 50/50 fiber couplers are usually slightly unbalanced, accurate image acquisitions require a preliminary calibration procedure of the collection system. It can be carried out by setting the polarization of the impinging collimated beam described above at 45° with respect to the orthogonal axis of the detection system. Then the projection of the input field onto the detection axis is directly measured with photodetectors D_1 and D_2. Ideally equal to 1, the ratio between the detected powers serves as the correction factor between the two polarizing channels for the following near-field acquisitions.

4. Vectorial Imaging of Radially Polarized Bessel Beams

Given the axial symmetry of its electric field, radial polarization is highly appropriate for focused-beam probing of the optical response of polarization-sensitive nanodevices such as single fluorophores [17] or nanoantennas [18]. The combination of these polarization states with propagative and evanescent Bessel beams offers the possibility for test-field distributions of high aspect ratio that can be described by a simple analytical expression (Bessel functions J_0 and J_1). The high aspect ratio relaxes the demands on probe positioning, whereas the simple field expressions allow obvious and straightforward comparison of the experimental and theoretical results. Since an arbitrary sample near zone can contain both propagative and evanescent waves, we choose to validate our microscope system through the imaging of radially polarized propagative and evanescent Bessel beams.

A. Propagative Bessel Beam

The Bessel field distribution is generated by projecting a collimated radially polarized beam [19] directly onto a conical lens or axicon [20] of a numerical aperture (NA) equal to 0.68. The tip is immersed in the Bessel beam zone and is scanned to accumulate the light field distribution in the beam's transverse plane (XY plane) perpendicular to its propagation direction (Z). The collected signal is subsequently analyzed in the multichannel polarizing system.

The vectorial structure of the transverse electric-field distribution as measured experimentally is shown in Figs. 2(a)–2(c) and is predicted theoretically in Figs. 2(d)–2(f) [21] (image size: 4 μm). Figures 2(a) and 2(d) display the overall transverse intensity distribution $|E_x|^2 + |E_y|^2$ (given experimentally by channel 3; see Fig. 1); Figs. 2(b) and 2(e) report the intensities of the orthogonal transverse electric field component $|E_x|^2$ (channel 1) and Figs. 2(c) and 2(f) report the results for $|E_y|^2$ (channel 2). The Bessel beam central fringe is transformed into orthogonal two-grain structures when imaged with polarizing channels 1 and 2. These typical images are due to the axis symmetrical polarization state in the beam transverse plane. The good agreement between experimental images and theoretical predictions validates our multichannel SNOM system with regard to high resolution vectorial probing of low spatial frequency field distributions.

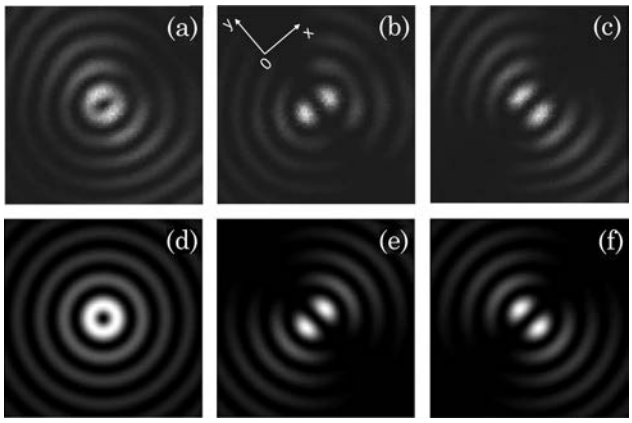

Fig. 2. (a)–(c) Bessel beam acquisitions through channels 3, 1, and 2, respectively. Simulation of the Bessel beam vectorial structure in the transverse plane: (d) intensity of the overall transverse electric field; (e), (f) intensity of the orthogonal transverse components E_x and E_y, respectively. Image size: 4 μm × 4 μm.

B. Evanescent Bessel Beam

To demonstrate the simultaneous detection of evanescent field components, we used the experimental setup depicted in Fig. 3. The evanescent Bessel beam is achieved with a 1.2 NA conical device composed of a solid immersion conical lens and a microaxicon engineered directly at the end of the fiber radial polarizer introduced previously (see Ref. [22]). The tip is scanned over the flat output interface of this refractive system. During the raster scan, the tip-to-surface nanometer distance is maintained with a conventional shear-force distance control setup. To ensure a satisfying signal-to-noise ratio, a conventional synchrone detection system is added to each of the three output channels of the microscope by modulating the input laser beam and inserting lock-in amplifiers ($L1$–$L3$ in Fig. 3) between the three detectors and the computer.

The vectorial structure of the radially polarized evanescent Bessel beam as measured experimentally is shown in Figs. 4(a)–4(c) and is simulated numerically as shown in Figs. 4(d)–4(f). Note that Figs. 4(a)–4(c)

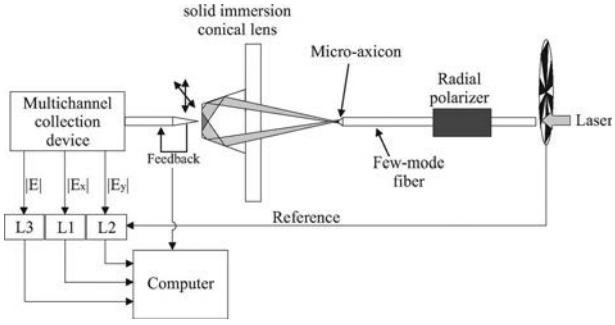

Fig. 3. Scheme of the experimental setup for the generation and vectorial characterization of a radially polarized evanescent Bessel beam.

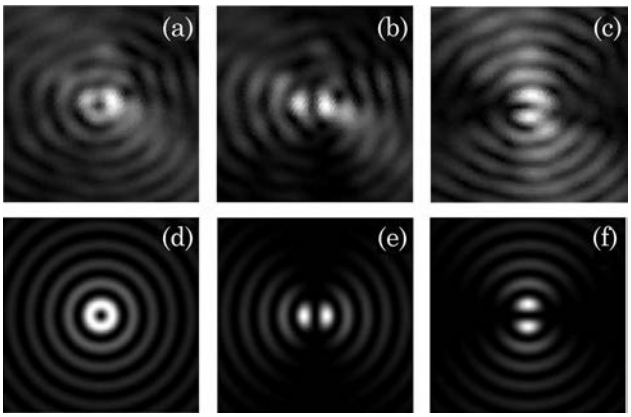

Fig. 4. (a)–(c) Evanescent Bessel beam acquisition through channels 3, ,1 and 2, respectively. Simulation of the Bessel beam vectorial structure in the transverse plane: (d) intensity of the overall transverse electric field; (e), (f) intensity of the orthogonal transverse components E_x and E_y, respectively. Image size: $2.7\,\mu\text{m} \times 2.7\,\mu\text{m}$.

are given by channels 3, 1, and 2, respectively. The overall transverse electric field intensity $|E_x|^2 + |E_y|^2$ is reported in Figs. 4(a) and 4(d); Figs. 4(b), 4(e), 4(c), and 4(f) show the intensity distributions of the orthogonal transverse electric field components ($|E_x|^2$ and $|E_y|^2$, respectively). The images are $2.7\,\mu$m.

Despite some discrepancies between the measured and the ideal beams that reflect the difficulty of synthesizing a perfectly ideal radially polarized evanescent Bessel beam, we see that these results validate our SNOM concept in the probing of pure evanescent fields. The typical highly asymmetric distributions of the transverse E_x and E_y field components simulated in Figs. 4(e) and 4(f) are clearly observed in the experimental images shown in Figs. 4(b) and 4(c). The nonuniformities in the experimental beam are assumed to be due to an asymmetry of the conical beam diffracted by the microaxicon and to slight misalignments between the interfaces of the overall conical refractive system. The usefulness of our multichannel polarization-sensitive SNOM introduced here, for either further improvements in the generation of this particular Bessel beam or in any other nano-optical system, is highly evident. We see from Fig. 4 that a fiber network of three output channels coupled with a dielectric uncoated tip provides an acceptable signal-to-noise ratio for SNOM applications.

5. Conclusion

We have introduced a concept of multichannel near-field fiber probe for the simultaneous imaging of optical field distributions with orthogonal polarizations (linear or elliptic). A first configuration of a three-channel probe has been proposed for the simultaneous and selective collection of two orthogonal components of the transverse electric field (parallel to the sample surface) as well as the overall transverse field (a combination of the two components). The system has been validated with the probing of both radially polarized propagative and evanescent Bessel beams. Recent advances in the probe design can provide the perspective for simultaneous and selective probing of both electric and magnetic field components. Our concept can be implemented in numerous collection-mode or reflection-mode near-field microscope configurations for a deeper insight of light polarization effects and vector fields at a subwavelength scale.

This research is funded by the Agence Nationale de la Recherche under contract ANR07-NANO-036, supported by the Pôle de compétitivité Microtechnique.

References

1. D. W. Pohl, W. Denk, and M. Lanz, "Optical stethoscopy: image recording with resolution $\lambda/20$," Appl. Phys. Lett. **44**, 651–653 (1984).
2. U. Fischer, U. T. Dürig, and D. W. Pohl, "Near-field optical scanning microscopy in reflection," Appl. Phys. Lett. **52**, 249–251 (1988).
3. D. Courjon, K. Sarayeddine, and M. Spajer, "Scanneling tunneling optical microscopy," Opt. Commun. **71**, 23–28 (1989).
4. R. Bachelot, P. Gleyzes, and A. Boccara, "Near-field optical microscope based on local perturbation of a diffraction spot," Opt. Lett. **20**, 1924–1926 (1995).
5. E. Betzig, J. K. Trautman, J. S. Weiner, T. D. Harris, and R. Wolfe, "Polarization contrast in near-field scanning optical microscopy," Appl. Opt. **31**, 4563–4568 (1992).
6. S. Bozhevolnyi, M. Xiao, and O. Keller, "External-reflection near-field optical microscope with cross-polarized detection," Appl. Opt. **33**, 876–880 (1994).
7. C. Adelmann, J. Hetzler, G. Scheiber, T. Schimmel, M. Wegener, H. B. Weber, and H. von Löhneysen, "Experiments on the depolarization near-field scanning optical microscope," Appl. Phys. Lett. **74**, 179–181 (1999).
8. E. Betzig, J. Trautman, R. Wolfe, E. Gyorgy, P. Finn, M. Kryde, and C.-H. Chang, "Near-field magneto-optics and high density data storage," Appl. Phys. Lett. **61**, 142–144 (1992).
9. T. Lacoste, T. Huser, R. Prioli, and H. Heinzelmann, "Contrast enhancement using polarization-modulation scanning near-field optical microscopy (PM-SNOM)," Ultramicroscopy **71**, 333–340 (1998).
10. L. Ramoino, M. Labardi, N. Maghelli, L. Pardi, M. Allegrini, and S. Patane, "Polarization-modulation near-field optical microscope for quantitative local dichroism mapping," Rev. Sci. Instrum. **73**, 2051–2056 (2002).
11. M. Burresi, D. van Oosten, T. Kampfrath, H. Schoenmaker, R. Heideman, A. Leinse, and L. Kuipers, "Probing the magnetic field of light at optical frequencies," Science **326**, 550–553 (2009).
12. S. Vignolini, F. Intonti, F. Riboli, D. S. Wiersma, L. Balet, L. H. Li, M. Francardi, A. Gerardino, A. Fiore, and M. Gurioli, "Polarization-sensitive near-field investigation of photonic crystal microcavities," Appl. Phys. Lett. **94**, 163102 (2009).
13. T. Grosjean and D. Courjon, "Polarization filtering induced by imaging systems: effect on image structure," Phys. Rev. E **67**, 046611 (2003).
14. T. Grosjean, M. Mivelle, and G. Burr, "Polarization-dependent extraction properties of bare fiber probes," Opt. Lett. **35**, 357–359 (2010).
15. A. Bouhelier, F. Ignatovich, A. Bruyant, C. Huang, G. C. des Francs, J.-C. Weeber, A. Dereux, G. P. Wiederrecht, and L. Novotny, "Surface plasmon interference excited by tightly focused laser beams," Opt. Lett. **32**, 2535–2537 (2007).
16. E. Bortchagovsky, G. C. des Francs, D. Molenda, A. Naber, and U. Fischer, "Transmission of an obliquely incident beam of

light through small apertures in a metal film," Appl. Phys. B **84**, 49–53 (2006).
17. L. Novotny, M. Beversluis, K. S. Youngworth, and T. G. Brown, "Longitudinal field modes probed by single molecules," Phys. Rev. Lett. **86**, 5251–5254 (2001).
18. T. Grosjean, A. Fahys, M. Suarez, D. Charraut, R. Salut, and D. Courjon, "Annular nanoantenna on fibre micro-axicon," J. Microsc. (Oxford) **229**, 354–364 (2008).
19. T. Grosjean, A. Sabac, and D. Courjon, "A versatile and stable device allowing the efficient generation of beams with radial, azimuthal or hybrid polarizations," Opt. Commun. **252**, 12–21 (2005).
20. R. Herman and T. Wiggins, "Production and Uses of Diffractionless Beams," J. Opt. Soc. Am. A **8** (6), 932–942 (1991).
21. Z. Bouchal and M. Olivik, "Non-diffractive vector Bessel beams," J. Mod. Opt. **42** (8), 1555–1566 (1995).
22. T. Grosjean, S. S. Saleh, M. A. Suarez, I. A. Ibrahim, V. Piquerey, D. Charraut, and P. Sandoz, "Fiber microaxicons fabricated by a polishing technique for the generation of Bessel-like beams," Appl. Opt. **46**, 8061–8067 (2007).